Underlayer-induced perpendicular magnetic anisotropy in ultrathin Co/Au/Cu(111) films: A spin-wave Brillouin-scattering study

Akihiro Murayama,* Kyoko Hyomi, James Eickmann, and Charles M. Falco

Optical Sciences Center and Surface Science Division of Arizona Research Laboratories, University of Arizona, Tucson, Arizona 85721

We have used spin-wave Brillouin scattering to study the perpendicular magnetic anisotropy of ultrathin Co/Au/Cu(111) films with various thicknesses of Au underlayer. From the field dependence of the spin-wave frequency we find that the second-order (fourth power) uniaxial perpendicular anisotropy increases monotonically with increasing Au-underlayer thickness ranging from 0 to 5 monolayers (ML), while the first-order (second power) anisotropy shows a nonmonotonic increase with a minimum at 1 ML Au. The ratio of the second-order anisotropy constant to the first one also increases with increasing Au thickness, from 0.01 to 0.07. We observe saturation for both the perpendicular anisotropy constants for a 5 ML Au underlayer, which coincides with saturation of expansion of the in-plane Co lattice due to the coherent growth of Co at the interface between the Co and Au underlayer. When the thickness of Au is further increased beyond 5 ML, we find an anisotropy-independent increase in coercivity on the polar-Kerr hysteresis curves. We also have observed a field-dependent broadening of the spin-wave Brillouin spectrum around a critical field between out-of-plane and in-plane magnetizations, which we explain by assuming a distribution of the first-order perpendicular anisotropy. As the result, the normalized distribution of the first-order anisotropy is shown to have a minimum at 1 ML Au thickness. We believe the observed Au-thickness dependences of the perpendicular anisotropy and of the distribution are characteristic behaviors due to an atomic-scale transition of the underlayer materials from Cu to Au. [S0163-1829(98)07237-3]

I. INTRODUCTION

Magnetic anisotropy in ultrathin films and superlattices is of considerable interest, since the contribution of the multiple surfaces and interfaces to the anisotropy is important in those artificial structures.[1] Uniaxial perpendicular anisotropy can be as high as 10^7 erg/cm^3 in superlattices composed of Co and nonmagnetic transition metals such as Pd, Pt, and Au. Because of this, studies of these materials are of interest both for fundamental understanding of magnetism, as well as for potential applications in ultrahigh density magnetic recording. Experimental studies on the material dependence,[2] and the effect of crystal symmetry,[3] as well as theoretical work based on the electronic structure, have been previously presented.[4] In addition, the characteristic dependence of the perpendicular anisotropy on the thickness of the nonmagnetic transition-metal overlayer has been studied.[5,6] A sharp maximum in the anisotropy was found for an overlayer thickness of 1 monolayer (ML) and the maximum also has been observed using different overlayer materials, including Cu, Ag, Au, and Pd. This latter observation suggests an effect of electronic structure, rather than an effect of strain, since the lattice constants of those overlayer materials are significantly different. Another experiment found that the perpendicular anisotropy in Co grown on an Au-underlayer has a minimum at 1 ML of the Au.[7] This effect is opposite to the overlayer-thickness dependence of the perpendicular anisotropy. These anomalous behaviors of the perpendicular anisotropy show that detailed studies of ferromagnetic single layers stacked with transition-metal layers are needed for a better understanding of the effects of atomic-scale interfaces

on the anisotropy. Thus far Co films stacked with relatively thick Au films have been extensively investigated, as a typical material-combination exhibiting a large perpendicular anisotropy.[8,9] However, even in the Co/Au system, studies with varying thickness of Au, which significantly affects the strain in the Co,[10] have not yet been sufficiently conducted.

In this article, we report detailed spin-wave Brillouin-scattering studies of the Au-underlayer dependence of the uniaxial perpendicular anisotropy in molecular-beam-epitaxy (MBE) -grown Co/Au/Cu(111) single-crystal films. The spin-wave energy of a surface mode observed in a typical Brillouin experiment is sensitive to the surface anisotropy.[11] The spin-wave frequency in 3-ML-thick Fe single layers with a strong perpendicular anisotropy has been quantitatively examined as a function of external field and the contribution of the second-order (fourth power) perpendicular anisotropy has been pointed out.[12] *In situ* Brillouin measurements have studied the effect of a Cu overlayer on the surface anisotropy in Co(001)/Cu ultrathin films.[13] Recently, the contribution of tetragonal misfit strain to a crystalline anisotropy has been investigated in fcc Co(110)/Cu.[14] However, in contrast with those lattice systems, the uniaxial perpendicular anisotropy in an ultrathin Co(0001) or Co(111) single layer with sixfold symmetry has not been examined sufficiently. As well as reporting our measurements, this paper discusses the physical origin of the Au-thickness dependence of the perpendicular anisotropy observed based on our structural analysis. In addition, we show that the spin-wave Brillouin spectrum is sensitive to magnetic inhomogeneities that depend on the Au underlayer in those Co films. Also, the distribution of perpendicular anisotropy is derived from the field dependence of the spin-wave spectrum width.

II. EXPERIMENT

Films were deposited in our modified Perkin-Elmer MBE system[6] under ultrahigh vacuum (UHV) conditions with a base pressure better than 1×10^{-10} Torr. Single-crystal Si(111) wafers of diameter 76 mm were cleaned using hydrogen fluoride and used as substrates. The Si substrates were annealed at 750 °C under UHV to show a 7×7 reconstructed surface. A 4.00-nm-thick Cu-buffer layer was deposited after cooling the substrate to room temperature. After depositing the Cu-buffer layer, two types of Au underlayers were prepared. One type was a step-wedged Au underlayer with thicknesses ranging from 0 to 3.2 ML and with the length of 8.9 mm for each step fabricated using a computer-controlled step-movable shutter. This method allowed us to make ultrathin Au films with various thicknesses under identical deposition conditions. Another type of Au underlayer was a continuous wedge with graded thickness from 1 to 20 ML. This wedge increased in thickness by 1 ML every 3 mm, with the length of 3 mm chosen to be much larger than the 0.1 mm diameter light spot used in the Brillouin measurements. After deposition of wedged Au underlayers, single Co films with thicknesses of 5 ML (for the step-wedged Au) and 6 ML (for the continuous wedge) were grown. As shown latter, these thicknesses of the Co layers were carefully chosen to be appropriate for the observation of the transition between in-plane and out-of-plane magnetizations with varying external field. Finally, an Au overlayer of 3.50 nm was deposited to prevent oxidation of the Co. The Au and Co films were all deposited at room temperature. Electron-beam evaporators controlled by optical-feedback monitors were used for the depositions with rates of 0.04 nm/s (Cu), 0.01 nm/s (Au), and 0.01 nm/s (Co), respectively, which were determined with an absolute accuracy within $\pm 10\%$ using Rutherford backscattering spectroscopy (RBS). The thickness distribution for the wedge samples on the 76 mm diameter substrate was within 5% of the designed thickness, without substrate rotation. Substrate rotation during the deposition of the Cu-buffer layer, Co, and Au overlayer assured thickness variations less than 1%. Those thickness distributions also were determined by RBS.

To evaluate the film quality and structure, reflection high-energy electron diffraction (RHEED) and Auger electron spectroscopy (AES) were used *in situ*. Films for the RHEED analysis were deposited using planar, rather than wedged, Au underlayers, since our experimental setup did not allow us to focus the electron beam of RHEED on each ML step of the Au underlayer. During the deposition, RHEED images were digitized using a CCD camera and captured by a computer. Each image was taken at a time interval of 7 s, which corresponded to a thickness resolution of 0.3 ML. To check the chemical purity of the Co layers, AES was used on Co films with various thicknesses ranging from 3 to 9 ML on a Au/Cu/Si(111) surface. This sample allowed us to analyze the thickness dependence of the film quality of the Co, instead of using a depth profiling technique with ion irradiation with the resultant heavy interface mixing.

After growth of films, we measured *ex situ* Brillouin light scattering to study the spin-wave spectrum in those Au/Co/Au/Cu/Si(111) samples. The excitation light source was the linear- and vertical-polarized single mode of a diode-pumped and frequency-doubled Nd:YAG laser with emission wavelength of 532 nm and with output power of 200 mW. A backscattering geometry was used to collect the inelastic polarized-scattered light normal to the incident vertical mode, which allowed us to detect only the scattering light due to the spin waves. An incident angle of the laser light and a collecting angle of the scattering from the sample surface were 45 degrees. A tandem six-pass $(3+3)$ Fabry-Perot interferometer and a solid state detector with quantum efficiency of 44% and dark count of 2.2 cps were used for the detection of the spin-wave spectrum. Instrumental spectrum width was measured to be 0.5 GHz. An external magnetic field was applied up to 11.6 kOe parallel to the film plane and normal to the polarization of the incident laser light. In addition to this Brillouin measurement, *ex situ* polar-Kerr hysteresis curves were measured using external fields up to 10 kOe.

III. RESULTS AND DISCUSSION

A. Film growth and structure

For Cu-buffer layers deposited without substrate heating RHEED indicates a structural transformation from Cu silicide[15] with poor crystallinity into a well defined fcc-(111) plane at a coverage of 1.5 nm. RHEED patterns then show narrow streaks for Cu-buffer layers thicker than 1.5 nm, as well as for the Au underlayer, Co, and Au overlayer. These results indicate that the fcc-(111) structure with high crystallinity and flat surface is epitaxially grown through each of the layers. A rotation of 30 degrees around the [111] axis is observed between the Si substrate and the Cu-buffer layer, which agrees with a previous result obtained by transmission electron microscopy.[15] It should be noted that in our RHEED analysis it is difficult to specify the stacking faults and distinguish possible hcp-(0002) stacking from fcc-(111) stacking of the ultrathin Co single layer. Previous work has shown that after forming the Cu fcc-(111) surface an average lattice constant of the Au layer on the Cu-buffer layer increases monotonically with increasing Au thickness ranging from 0 to 5 ML, at which point it has reached the bulk value.[10] We find that the Co growth on this Au underlayer is coherent at the interface, and that the lattice constants of Co layers are expanded by the Au underlayer. Hence, the lattice expansion of Co layers also saturates with the 5-ML-thick Au underlayer. The strain in Co is maximum at the Co/Au interface and relaxes gradually as the Co thickness increases. An example of these features is shown in Fig. 1, taken from quantitative measurements of the in-plane lattice spacing. The intensity of the specular diffraction from the Co layer is relatively low at the beginning of the deposition and increases gradually with increasing Co thickness. Oscillations in intensity of the specular beam are not observed during the film growth of Co on Au underlayers. We note that our previous RHEED analysis showed that Au growth on Co was incoherent and stress free for Au coverages larger than 1 ML.[6]

In AES analysis, the intensity ratios of the Co to the Au underlayer as well as to the Cu of the buffer layer increase monotonically with increasing Co thickness. Moreover, we cannot see any signal from the *LMM* or *KLL* transition of Si in our Co films. Hence, we conclude that any contamination
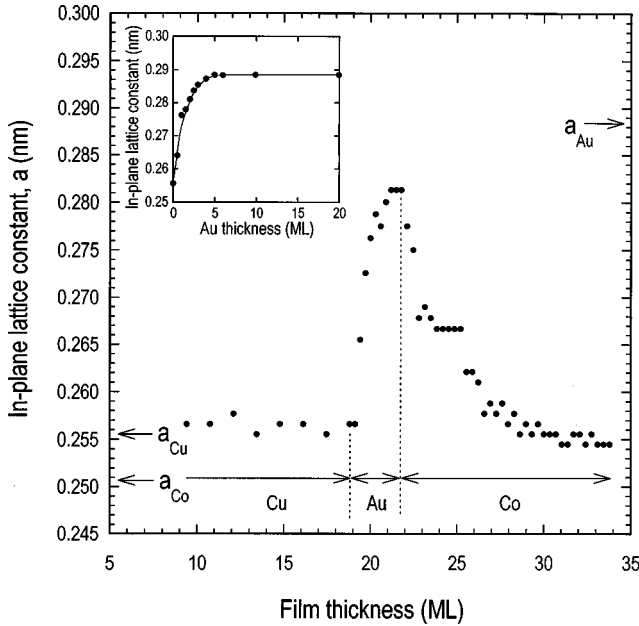
FIG. 1. In-plane lattice constant obtained from intensity line scans of RHEED images as a function of film thickness, with a 3.2 ML Au underlayer. Materials deposited are indicated on the figure. The lattice constant is calibrated by the lattice spacing of the Si(7 ×7) substrate surface. In the inset, the lattice constant of the Au-underlayer surface is shown as a function of the Au-underlayer thickness. The bulk metal lattice spacings are $a_{Cu} = 0.2556$ nm, $a_{hcp-Co} = 0.2507$ nm, and $a_{Au} = 0.2884$ nm, respectively. The lattice spacings quoted are for room temperature (295 K).

of Au, Cu, or Si into Co magnetic layers is negligible, in our films deposited without intentional substrate heating.

B. Step-wedged Au underlayer with thicknesses from 0 to 3 ML

Figure 2 shows the spin-wave frequency as a function of the in-plane magnetic field for 5-ML-thick Co films with various thicknesses of the Au underlayer. The lowest uniform spin-wave mode was used for the fitting calculation, taking into account both the direction of the magnetization and the contribution of the second-order (fourth power) uniaxial perpendicular anisotropy.[12] In ultrathin ferromagnetic films, the energy of the uniform mode is very close to that of the surface mode which has a wave-number vector parallel to the film surface and is accessible by the excitation light. In our Co/Au/Cu(111) films, the spin-wave frequency is found to be independent of the angle between the in-plane crystal axis and the applied field. This indicates directly that the effect of the in-plane anisotropy field on the spin-wave frequency is less than our 0.5 GHz instrumental spectrum width. Hence, the in-plane crystal anisotropy is omitted in the following calculation. The first and second terms of uniaxial anisotropy constants, $K_u^{(1)}$ and $K_u^{(2)}$, are included in the free energy per unit of the system, as follows:

$$E = -HM_s \cos \alpha + (2\pi M_s^2)$$
$$\times \sin^2 \alpha - K_u^{(1)} \sin^2 \alpha - K_u^{(2)} \sin^4 \alpha. \quad (1)$$
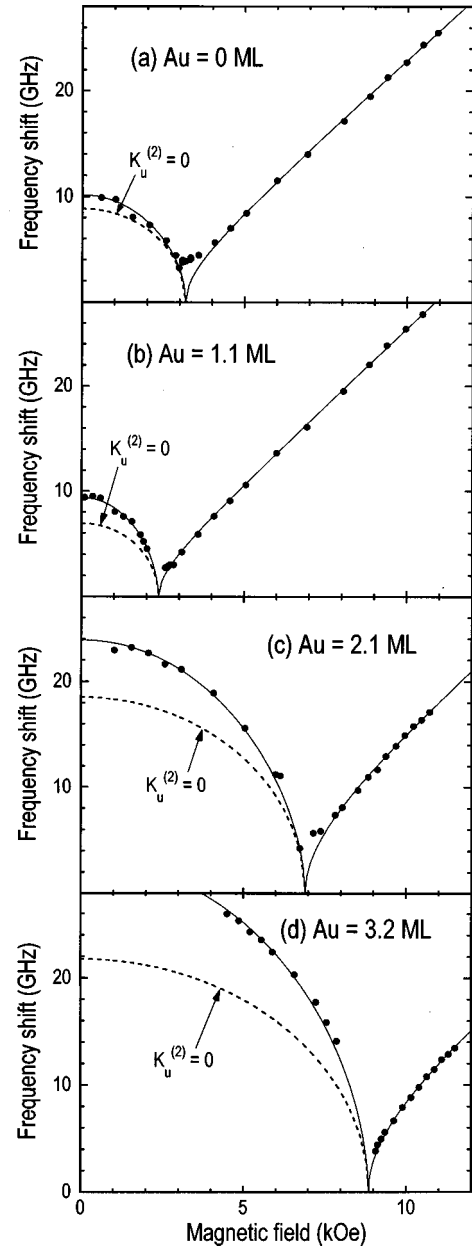

FIG. 2. Magnetic-field dependence of the spin-wave frequency in 5 ML Co films for various thicknesses of the Au underlayer. Solid line is the calculated best fit. Dotted line is a calculation made without a $K_u^{(2)}$ term [see Eq. (1)].

The external field H is applied along the film plane and α is the angle of the saturation magnetization M_s with respect to the film plane. In this definition, a positive value of each anisotropy constant indicates a preferred perpendicular orientation for the magnetization. The equilibrium position of the M_s is derived by taking the angular differential of Eq. (1). An effective magnetization density is also introduced as

$$(4\pi D_\perp M_s)_{eff} = 4\pi D_\perp M_s - 2K_u^{(1)}/M_s, \quad (2)$$

where $D_\perp$, the effective demagnetizing factor, is equal to 1 for a 5-ML-thick fcc-(111) or hcp-(0001) plane.[16-18] If the effective magnetization density is negative, M_s is oriented perpendicular to the film plane in zero applied field. How-

TABLE I. Results of the best fitted calculations for the field dependence of spin-wave Brillouin frequency, in 5-ML-thick Co films with various thicknesses of Au underlayers. Coercivity on polar-Kerr hysteresis curves is also listed.

Au underlayer Thickness (ML)	Polar-Kerr Coercivity (Oe)	g factor	Spin-wave Brillouin scattering					
			$(4\pi D_\perp M_S)_{eff}$ (kOe)	$2K_u^{(2)}/M_S$ (kOe)	$K_u^{(1)}$ (10^7 erg/cm^3)	$K_u^{(2)}$ (10^6 erg/cm^3)	$K_u^{(1)}+K_u^{(2)}$ (10^7 erg/cm^3)	$K_u^{(2)}/K_u^{(1)}$
0	192	1.98	-3.19	0.12	1.50	0.17	1.52	0.011
0.5	106	2.09	-2.15	0.24	1.42	0.34	1.45	0.024
1.1	95	2.09	-2.43	0.19	1.44	0.27	1.47	0.019
1.6	105	2.01	-5.15	0.32	1.64	0.46	1.69	0.028
2.1	122	1.94	-6.98	0.44	1.77	0.63	1.83	0.036
2.7	170	1.85	-8.23	0.80	1.86	1.10	1.97	0.059
3.2	220	1.76	-8.86	0.94	1.90	1.30	2.03	0.068

ever, for applied fields larger than $|(4\pi D_\perp M_s)_{eff}|$ the magnetization is oriented parallel to the external field in the film plane.

The spin-wave frequency is obtained using the general equation derived by Smit and Belgers[19] and the field dependence of the spin-wave frequency in each sample can be entirely explained by this fitting. We also have attempted to evaluate the effects of both dipole and exchange fields on the spin-wave frequency in the ultrathin Co film, which are caused by fluctuations of the magnetization due to the spin-wave excitation observed using this light-scattering method. For this purpose, we modified the spin-wave theory assuming in-plane magnetization,[20] to be applicable for films having out-of-plane magnetization due to a uniaxial perpendicular anisotropy. In a Co film of thickness only 5 ML, the contribution of the dipole field to the spin-wave frequency is in the range 0.1–0.5 GHz, which depends on the external field and the effective magnetization. Also, the exchange contribution is below 0.1 GHz. These results justify neglecting the dipole and exchange effects on the spin-wave energy in the fitting procedure described above. In films without the Au underlayer, the spin-wave frequency tends to be constant at 4 GHz around the critical field, which indicates the effect of domain formation should be considered. Although below the critical field, the formation of stripe-type domains might be possible even in these ultrathin Co films, there is no experimental evidence from our fitting results to support an effect of domain formation on the spin-wave energy.

Results of our calculations of spin-wave frequencies are listed in Table I. Also listed are coercivities H_c determined from polar-Kerr hysteresis curves. H_c shows a minimum at a Au thickness of 1 ML. Using a vibrating sample magnetometer (VSM) having low circuit noise and with samples cut into 8×8 mm^2, we have confirmed directly that within $\pm 5\%$ the values of M_s are 1370 G for our 5-ML-thick Co single layers with various thicknesses of Au underlayer. Since this is comparable with that of pure Co, the bulk value of 1422 G is used for the calculation of the anisotropy constants. The first and second terms of perpendicular anisotropy, $K_u^{(1)}$ and $K_u^{(2)}$, are shown in Fig. 3, as a function of Au thickness. As can be seen, $K_u^{(1)}$ shows a minimum anisotropy for an Au thickness near 1 ML. This result agrees with our previous measurement of a total perpendicular anisotropy in this stacking system, in which a polar-Kerr hysteresis technique with an external field parallel to the hard magnetization di-

rection was used.[7] In contrast, $K_u^{(2)}$ shows a monotonic increase with increasing Au thickness, rather than a minimum as seen in $K_u^{(1)}$. As shown in Table I, the ratio between $K_u^{(1)}$ and $K_u^{(2)}$ shows a monotonic increase from 0.01 to 0.07 with increasing Au thickness, remaining much smaller than the value of 0.4 characteristic of bulk hcp-Co. The g factor obtained from our fitting procedure shows a maximum of 2.09 around 1 ML of Au, which is close to the 2.2 of bulk Co. Previously, the effect of a strong perpendicular anisotropy on the g factor was observed in a Brillouin-scattering experiment on a Fe/Cu(001) sample.[12] In that experiment, a value
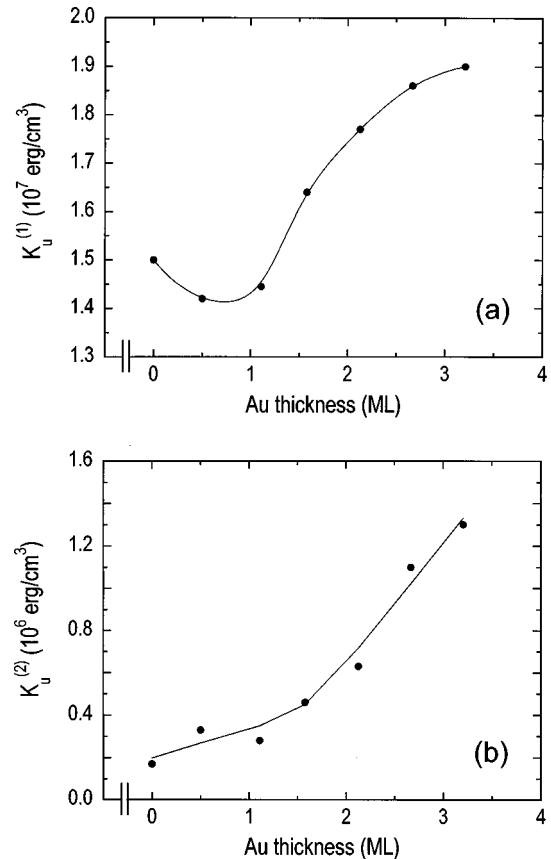

FIG. 3. Perpendicular magnetic anisotropy constants $K_u^{(1)}$ (a) and $K_u^{(2)}$ (b) as a function of the Au-underlayer thickness determined from fitting the data using Eq. (1) for the angular dependence of the magnetic free energy. Solid lines are guides for the eye.
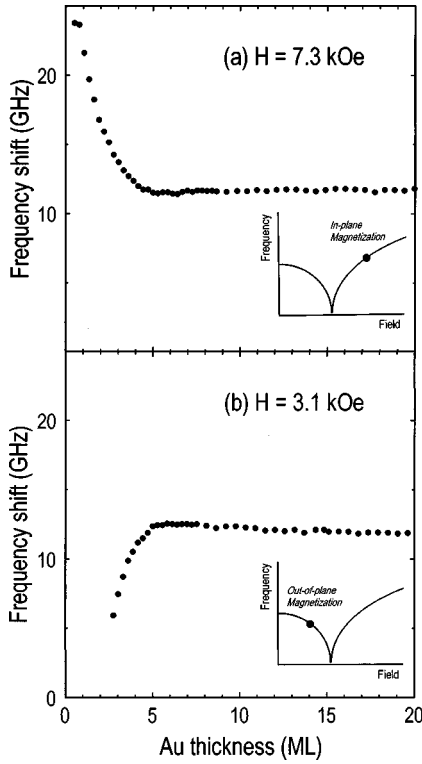
FIG. 4. Spin-wave frequency vs the Au-underlayer thickness for a 6 ML Co film deposited on a gradual wedge of Au underlayer. External fields of 7.3 kOe (a) and 3.1 kOe (b) were applied parallel to the film surface in order to maintain the magnetization in-plane and out-of-plane, respectively.
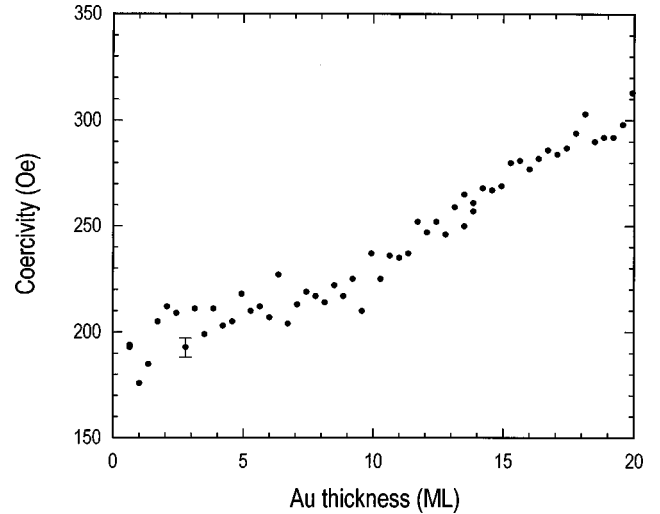

FIG. 5. Coercivity obtained from polar-Kerr hysteresis curves vs the Au underlayer thickness in 6 ML of Co. Au thicknesses were varied using a gradual-wedged Au underlayer.

of $g = 1.84$ was obtained. In our experiments, on ultrathin Co samples with a range of anisotropies the g factor appears to be well correlated with the value of $K_u^{(1)}$ as well as with the total perpendicular anisotropy $K_u^{(1)} + K_u^{(2)}$.

C. Continuous wedge Au underlayer

Figure 4 shows spin-wave frequencies as a function of the Au underlayer thickness in a gradual-wedge sample with 6 ML of Co. With an applied field of 7.3 kOe, the magnetization is in-plane and the spin wave on the upper branch above the critical field can be observed. Hence, this spin-wave frequency depends on the g value and effective magnetization field. Decreasing the Au thickness below 5 ML causes the spin-wave frequency to increase, which we showed in the previous section originates from an decrease in $K_u^{(1)}$ and a increase in the g value. The spin-wave frequency saturates for Au thicknesses greater than 5 ML. This saturation directly indicates the saturation of $K_u^{(1)}$ and of the resultant g value, since the M_s does not change with the Au thickness. Moreover, this saturation coincides with the saturation of the in-plane lattice expansion of Co at 5 ML of Au, as described earlier in Sec. III A. With a field of 3.1 kOe, in which the spin-wave frequency depends on both $K_u^{(1)}$ and $K_u^{(2)}$, saturation of the spin-wave frequency at 5 ML of Au is also observed in Fig. 4. On the lower branch of the spin wave for fields below the critical field, the change in the spin-wave frequency below 5 ML of Au is directly related to the change in $K_u^{(1)}$ and $K_u^{(2)}$. These results are confirmed by fitting cal-

culations for the field dependence of spin-wave frequency in this gradual wedge sample for Au thicknesses of 4, 5, and 20 ML. Therefore, we conclude that the increases of both $K_u^{(1)}$ and $K_u^{(2)}$ above 1 ML of Au are dominated by magnetoelastic effects due to the coherent growth of Co at the Co/Au interface.

Values of the coercive field, H_c as a function of the Au thickness, derived from polar-Kerr hysteresis curves, are shown in Fig. 5. As can be seen, H_c gradually increases with increasing Au thickness, showing no signs of saturation above 5 ML. This Au-underlayer dependence of H_c cannot be explained by the Au thickness dependence of the perpendicular anisotropies measured in our spin-wave experiments. Therefore, pinning and/or nucleation effects on domain motion in the magnetization reversal process should be taken into account. Such domain formation effects in the magnetization reversal was observed in an Au/Co/Au sandwich film with 3-nm-thick Au films.[21] Detailed structural analyses including an observation of the surface morphology of the Au underlayer are necessary for a full understanding of the increase in the H_c with Au thickness.

D. Field-dependent width of spin-wave Brillouin spectrum and magnetic inhomogeneity

As can be seen from Fig. 6, the spectrum width $\Delta\omega$ exhibits a field-dependent line broadening of the spin-wave Brillouin spectrum at the critical field for which the equilibrium magnetization lies just in-plane. This behavior is quantitatively explained by assuming a distribution of the effective magnetization fields, as follows:

$$\Delta\omega = \Delta\omega_0 + \Delta(4\pi D_\perp M_s)_{\text{eff}}\{\partial\omega/\partial(4\pi D_\perp M_s)_{\text{eff}}\}, \quad (3)$$

where ω is the observed spin-wave frequency. In this calculation the value of $(4\pi D_\perp M_s)_{\text{eff}}$ determined from the field dependence of the spin-wave frequency is used. Here, $\Delta\omega_0$ indicates the field-independent width due to structural inhomogeneities and $\Delta(4\pi D_\perp M_s)_{\text{eff}}$ is the distribution of effective magnetization fields, that is, the distribution of $K_u^{(1)}$ val-
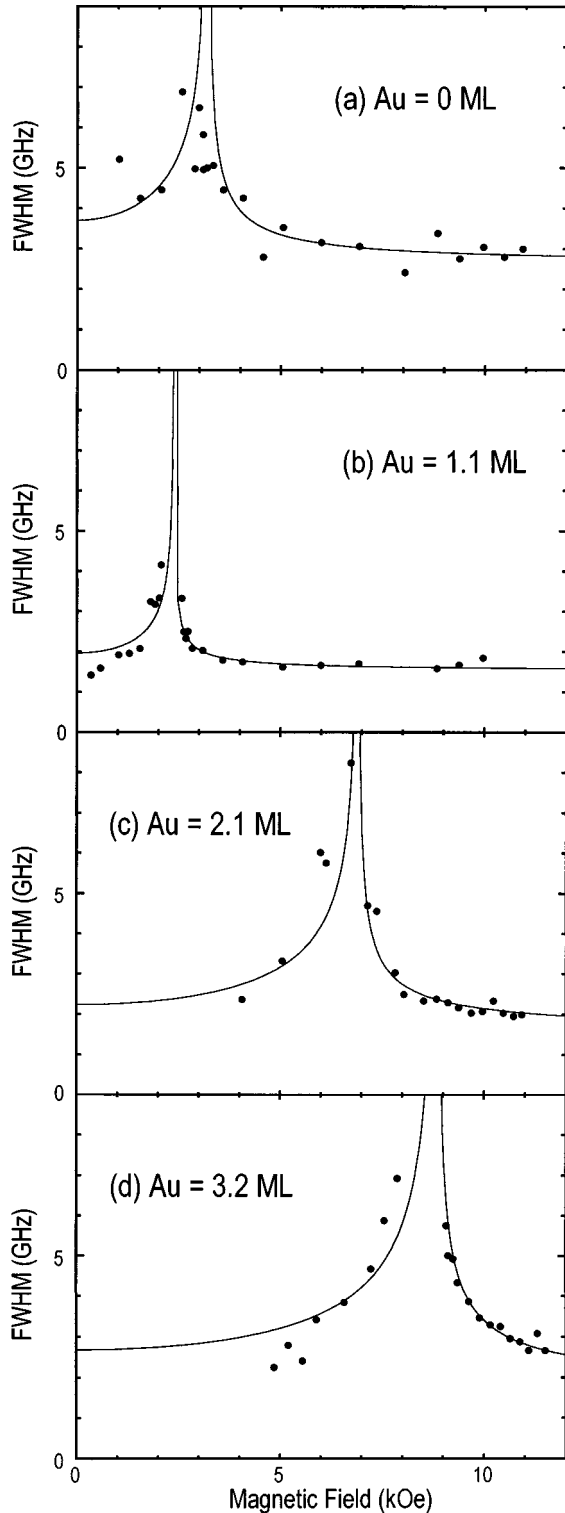
FIG. 6. Magnetic-field dependence of full width at half maximum (FWHM) of a spin-wave Brillouin spectrum for 5 ML Co films with various thicknesses of Au underlayer. Solid lines are the best fit calculations (see text).
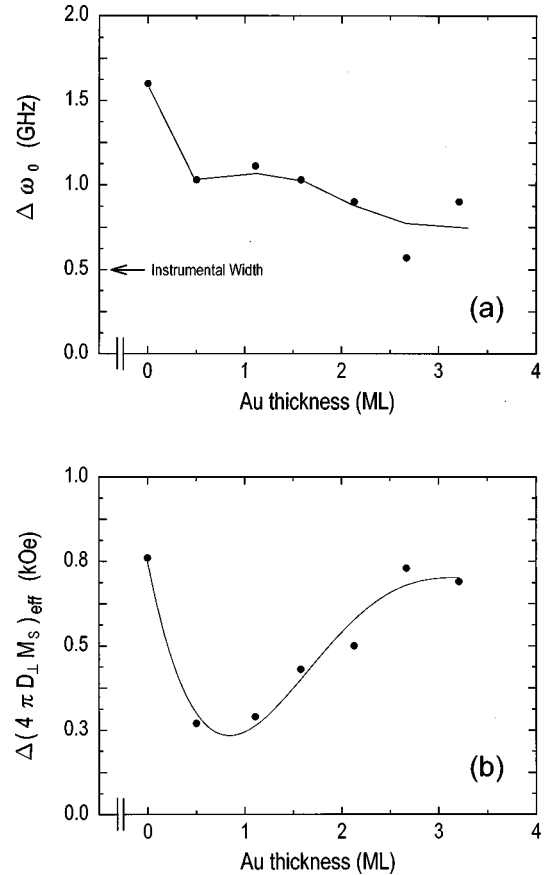

FIG. 7. Field-independent spectrum width $\Delta\omega_0$ (a), and the parameter $\Delta(4\pi D_\perp M_s)_{eff}$ (b) as a function of the Au-underlayer thickness. The latter parameter characterizes the inhomogenious distribution of the perpendicular anisotropy. These parameters were determined from a fitting calculation for the field-dependent line broadening of the spin-wave Brillouin scattering (see text). Solid lines are guides for the eye.

ues. Since we have confirmed that M_s has the bulk value independent of the Au-underlayer thickness, and the thickness distribution of planar Co deposited is within 1%, $\Delta(4\pi D_\perp M_s)_{eff}$ is mainly caused by the distribution of $K_u^{(1)}$. As can be seen from the solid lines in Fig. 6, the calculation

agrees very well with the data, especially above the critical field. Below the critical field, the scattering light intensity is considerably lower than that above the critical field due to the out-of-plane magnetization,[22] and thus measurement of the experimental width becomes less accurate. Also, in the sample without an Au underlayer, the effect of domain formation may decrease the spectrum width at the critical field. As shown in Fig. 7, we find that the parameters of $\Delta\omega_0$ and $\Delta(4\pi D_\perp M_s)_{eff}$ depend strongly on the thickness of the Au underlayer in our single-crystal films. Inserting only a 0.5 ML-thick Au underlayer results in a significant reduction of both $\Delta\omega_0$ and $\Delta(4\pi D_\perp M_s)_{eff}$.

The reduction of $\Delta\omega_0$, the field-independent line width, with increasing Au thickness indicates a marked improvement in the structure-related magnetic uniformity of the Co layer.[23] In the Co/Cu/Si(111) system, the Co was reported to show hcp-(0002) stacking.[24] On the other hand, superlattice samples of Co/Cu(111) showed fcc-(111) structure with small amounts of hcp,[25] while hcp-(0002) was identified in Co/Au(111) superlattices.[26] Hence, the structure of Co grown on Cu(111) grown without heating is unstable and is assumed to have considerable stacking faults. However, it appears from our measurements that these stacking faults are

eliminated by the ultrathin Au interlayer and that the hcp-(0002) planes are stabilized. This interpretation agrees with our experimental result that the spectrum width $\Delta\omega_0$ in Co/Cu(111) films does not depend on the Co thickness, at least in the range from 4 to 11 ML, since the density of stacking faults does not significantly depend on the thickness. Other structural imperfections, such as the island formation, should depend on the Co thickness.

The Au-thickness dependence of $\Delta(4\pi D_\perp M_s)_{\text{eff}}$ in the bottom curve of Fig. 7 indicates that the distribution of perpendicular anisotropy $K_u^{(1)}$ is strongly affected by the Au thickness. From the angular dependence of the absorption width in ferromagnetic resonance (FMR) measurements, the anisotropy distribution due to the dispersion of c-axis crystallites was obtained in polycrystalline Co films sandwiched by Au.[27] Also, the angular dependence of FMR line broadening was used to determine variations in the perpendicular effective field from in Fe(001)/Cu films.[28] It should be noted that the anisotropy distribution discussed here is obtained from a relatively microscopic area less than 100 μm in diameter, which is meaningfully less than the film area used in a standard microwave FMR experiments. As can be seen from Fig. 7, a decrease in the $\Delta(4\pi D_\perp M_s)_{\text{eff}}$ occurs for a 0.5 ML Au-underlayer thickness in our single-crystal films and coincides with an abrupt decrease in $\Delta\omega_0$. Therefore, we attribute this reduction of the anisotropy distribution to a significant elimination of stacking faults and possibly of the reduction in contamination by a fcc-(111) phase. However, the increase in $\Delta(4\pi D_\perp M_s)_{\text{eff}}$ with increasing Au thickness above 0.5 ML does not agree with the behavior of $\Delta\omega_0$, which will be discussed later.

E. Discussion

To evaluate the contribution of underlayer-induced strain to the uniaxial perpendicular anisotropy in the Co films, we estimate a total perpendicular anisotropy $K_u^{(\text{Total})}$ using a magnetocrystalline anisotropy K_{MC}, a magnetoelastic anisotropy K_{ME}, and a shape anisotropy, as follows:

$$K_u^{(\text{Total})} = K_{\text{MC}} + K_{\text{ME}} - 2\pi M_s^2. \tag{4}$$

The magnetoelastic anisotropy for Co(0002) film is calculated from

$$K_{\text{ME}} = -[C_{11} + C_{12} - 2(C_{13})^2/C_{33}](\lambda_A + \lambda_B)\varepsilon, \tag{5}$$

where C_{ij} is an elastic constant and λ is a magnetostriction constant.[25] Since the in-plane strain ε in Co depends on the Co thickness, we use strain values obtained from RHEED measurements of the actual lattice spacing of 5-ML-thick Co. Two values of K_{MC} are used in the calculation: one is the sum of the first- and second-order crystalline anisotropy of bulk hcp-Co, another is the first-order anisotropy of bulk hcp-Co. The reason to refer to the latter value is that the second-order anisotropy is experimentally shown to be several % of the first one. Additional strain due to the upper interface between Co and Au is not considered, since the growth of the Au overlayer on the Co was shown to be incoherent and stress free.[6] The result of this calculation is
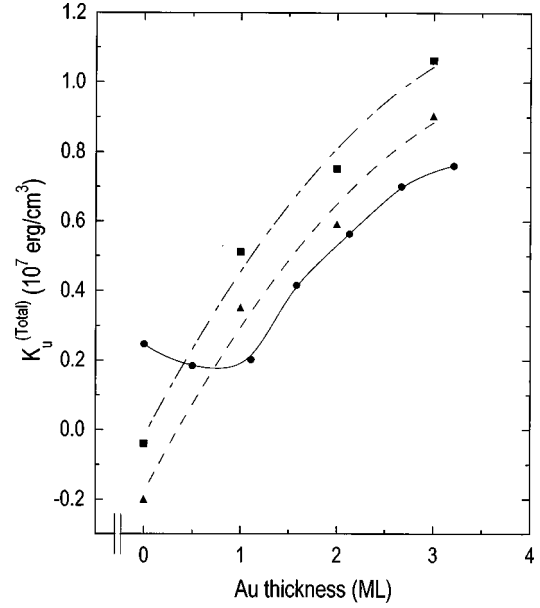

FIG. 8. Total anisotropy vs the Au-underlayer thickness. Closed circles are experimental values obtained from anisotropy constants $K_u^{(1)}$ and $K_u^{(2)}$, using $K_u^{(\text{Total})} = K_u^{(1)} + K_u^{(2)} - 2\pi M_s^2$. Closed squares are calculated values using $K_u^{(\text{Total})} = K_{\text{MC}} + K_{\text{ME}} - 2\pi M_s^2$, where the magnetoelastic anisotropy K_{ME} is evaluated based on the actual in-plane strain determined from RHEED images and the sum of the first- and second-order crystalline anisotropy of bulk hcp-Co is used for the crystalline anisotropy K_{MC}. Closed triangles are calculated values using K_{MC} without the second-order anisotropy (see text). Dotted and solid lines are guides for the eye.

compared with experimental values determined from our spin-wave experiment in Fig. 8. Here, the experimental value of $K_u^{(\text{Total})}$ is plotted, where

$$K_u^{(\text{Total})} = K_u^{(1)} + K_u^{(2)} - 2\pi M_s^2. \tag{6}$$

For values of $K_u^{(\text{Total})} > 0$, the anisotropy energy favors a perpendicular orientation for the magnetization density rather than an in-plane orientation, and the resulting easy axis of the magnetization is perpendicular to the film plane. There are two minimum energy states for a perpendicular magnetization and an in-plane magnetization. The system can reach the lowest energy state via incoherent rotation through the potential barrier between these minimum energy states. As can be seen from Fig. 8, without the Au underlayer the calculated value of total anisotropy indicates in-plane easy-axis magnetization. This is a consequence of the lattice mismatch between Co and Cu being a relatively small 1%. However, the experimental value indicates perpendicular easy axis. Hence, it appears an additional interface perpendicular anisotropy at the lower Co/Cu and upper Au/Co interfaces may sustain the perpendicular total anisotropy observed. For Au underlayers thicker than 1 ML, the Au-thickness dependence of the total anisotropy obtained experimentally qualitatively agrees with the calculated dependence. This is consistent with the increase in the perpendicular anisotropy above 1 ML of Au being mainly due to the magnetoelastic effect caused by the Au underlayer.

The transition region between Cu and Au underlayer is very interesting. In our structural analysis using RHEED, no anomalous effect in the Au-thickness dependence of the lattice spacing and specular beam intensity is observed around 1 ML of Au. As shown above, we observe abrupt decreases in $\Delta\omega_0$ and $\Delta(4\pi D_\perp M_s)_{eff}$ at 0.5 ML of Au, both showing marked improvement in the structural inhomogeneity and the anisotropy distribution. Therefore, we cannot attribute the minimum of $K_u^{(1)}$ to a degradation of K_{MC}, since the reduction of the stacking fault density or the elimination of a fcc-(111) phase should increase the perpendicular anisotropy in a single-crystal Co film. Other possible effects that could degrade the perpendicular anisotropy are interfacial mixing at the Co/Au interface and interfacial roughness due to poor wetting of Co on Au that is, island formation.[8] Additionally, hybridization of the electronic structure between Co and transition metals has been proposed as a possible mechanism to affect the interface anisotropy.[4,5,29] Since the role of the interface anisotropy on the total perpendicular anisotropy is important, and further investigation is in progress to elucidate the effect of the Au underlayer on this anisotropy.

Recently, a systematic study of Co/Mn superlattices revealed a structural transition from fcc-(111) to hcp-(0002) Co with increasing Mn thickness.[30] From the angular dependence of FMR fields, the contribution of $K_u^{(2)}$ was found to be negligible in the fcc phase, and the hcp phase in the 2.4-nm-thick Co superlattice was found to have the ratio of $K_u^{(2)}/K_u^{(1)}=0.05$. These results are consistent with our result that Co films deposited directly on Cu, which contain the fcc-(111) phase, have a small value of $K_u^{(2)}/K_u^{(1)}$. However, from the analysis of our Co/Au stacking system, we note that the effect of strain on the $K_u^{(2)}$ term should be taken into account for a full understanding of the Au-underlayer dependence of the ratio $K_u^{(2)}/K_u^{(1)}$.

Finally, we discuss the physical origin of the increase in the distribution of $K_u^{(1)}$ values with increasing Au thickness above 1 ML. The parameter $\Delta(4\pi D_\perp M_s)_{eff}$ characterizes the extent of the anisotropy distribution, which is the width of a steplike function describing the distribution. Hence, this value is independent of the intensity of the anisotropy. To clarify this point, in Fig. 9 we plot a normalized distribution of $K_u^{(1)}$ obtained from the value of $\Delta(4\pi D_\perp M_s)_{eff}$. A similar dependence on Au thickness of the normalized distribution $(\Delta K_u^{(1)}/K_u^{(1)})$ is exhibited by the variation of $\Delta(4\pi D_\perp M_s)_{eff}$ shown in Fig. 7. The distribution of perpendicular anisotropy can be related to the angular dispersion of the c axis of single-crystal Co. For example, from an analysis of x-ray data for Co/Pd superlattices, it was shown that the width of the rocking curves increased with increasing Co thickness, due to the large lattice mismatch between Co and Pd.[31] However, our RHEED results for Co/Au films show that sharp and narrow streak patterns are maintained throughout the deposition of Co. Also, the Co-thickness dependence of the RHEED intensity is similar for different thicknesses of Au. These results do not indicate a significant change in the dispersion of Co crystallite orientations and further efforts are necessary to elucidate the Au dependence of the Co lattice structure. On the other hand, nonuniform strain is a possible explanation for the increase in the anisotropy distribu-
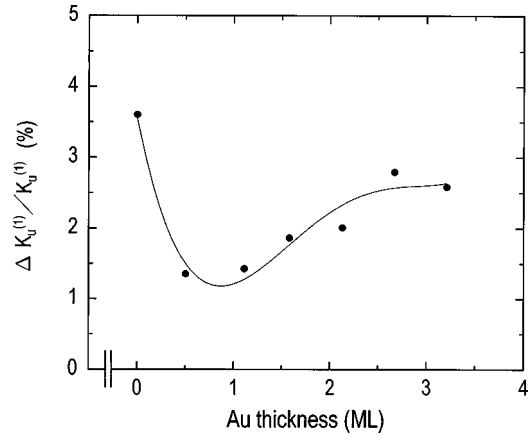

FIG. 9. Normalized anisotropy distribution $\Delta K_u^{(1)}/K_u^{(1)}$ obtained from $\Delta(4\pi D_\perp M_s)_{eff}$ as a function of the Au-underlayer thickness. The solid line is a guide for the eye.

tion, since the effect of strain on the perpendicular anisotropy becomes important above 1 ML of Au.

IV. SUMMARY

We have studied perpendicular magnetic anisotropy in ultrathin Co/Au(111) films with varying thicknesses of the Au underlayer by spin-wave Brillouin scattering. We explain the field dependence of the spin-wave frequency by a calculation that includes both the first- (second power) and second-order (fourth power) uniaxial perpendicular anisotropies. We find that the second-order perpendicular anisotropy increases monotonically with increasing Au-underlayer thickness ranging from 0 to 5 ML, while the first-order anisotropy shows a nonmonotonic increase with a minimum at 1 ML. The ratio of the second-order anisotropy constant to the first one is significantly less than the bulk value, and also increases with increasing Au thickness. Saturation of both the first- and second-order anisotropies for a 5 ML Au underlayer agrees well with the saturation of expansion of the in-plane Co lattice due to the coherent growth of Co at the Co/Au interface. Also, we observed a field-dependent broadening of the spin-wave Brillouin spectra around a critical field between out-of-plane and in-plane magnetizations. We interpret this broadening as due to a distribution of the first-order anisotropy depending on the thickness of Au underlayer. As a result, the distribution of the first-order anisotropy is shown to have a minimum at 1 ML of Au. The physical origins of the Au underlayer dependence of the perpendicular anisotropy and the distribution have been discussed mainly based on the structural analysis using RHEED.

ACKNOWLEDGMENTS

*Permanent address: R&D Division, ASAHI-KOMAG Co., Yon-ezawa, 992-11, Japan.

[1] See various articles in *Ultrathin Magnetic Structure I & II*, edited by B. Heinrich and J. A. C. Bland (Springer-Verlag, Berlin, 1994).

[2] F. J. A. den Broeder, W. Hoving, and P. J. H. Bloemen, J. Magn. Magn. Mater. **93**, 562 (1991).

[3] B. N. Engel, C. D. England, R. A. Van Leeuwen, M. H. Wied-mann, and C. M. Falco, Phys. Rev. Lett. **67**, 1910 (1991).

[4] A. J. Freeman and R. Wu, J. Magn. Magn. Mater. **100**, 497 (1991).

[5] B. N. Engel, M. H. Wiedmann, R. A. Van Leeuwen, and C. M. Falco, Phys. Rev. B **48**, 9894 (1993).

[6] B. N. Engel, M. H. Wiedmann, and C. M. Falco, J. Appl. Phys. **75**, 6401 (1994).

[7] B. N. Engel, C. Marliere, and C. M. Falco, IEEE Trans. Magn. **31**, 4080 (1995).

[8] F. J. A. den Broeder, D. Kuiper, A. P. van der Mosselaer, and W. Hoving, Phys. Rev. Lett. **60**, 2769 (1988).

[9] C. H. Lee, Hui He, F. J. Lamelas, W. Vavra, C. Uher, and Roy Clarke, Phys. Rev. B **42**, 1066 (1990).

[10] C. Marliere, B. N. Engel, and C. M. Falco (unpublished).

[11] B. Hillebrands, P. Baumgart, and G. Güntherodt, Phys. Rev. B **36**, 2450 (1987).

[12] J. R. Dutcher, B. Heinrich, J. F. Cochran, D. A. Steigerwald, and W. F. Egelhoff, Jr., J. Appl. Phys. **63**, 3464 (1988).

[13] P. Krams, F. Lauks, R. L. Stamps, B. Hillebrands, and G. Güntherodt, Phys. Rev. Lett. **69**, 3674 (1992).

[14] B. Hillebrands, J. Fassbender, R. Jungblut, G. Güntherodt, D. J. Roberts, and G. A. Gehring, Phys. Rev. B **53**, R10 548 (1996).

[15] C. S. Liu, S. R. Chen, W. J. Chen, and L. J. Chen, Mater. Chem. Phys. **36**, 170 (1993).

[16] B. Heinrich, S. T. Purcell, J. R. Dutcher, K. B. Urquhart, J. F. Cochran, and A. S. Arrott, Phys. Rev. B **38**, 12 879 (1988).

[17] M. Farle, A. Berghaus, and K. Baberschke, Phys. Rev. B **39**, 4838 (1989).

[18] M. Farle, A. Berghaus, Yi Li, and K. Baberschke, Phys. Rev. B **42**, 4873 (1990).

[19] J. Smit and H. G. Beljers, Philips Res. Rep. **10**, 113 (1955).

[20] J. F. Cochran, J. Rudd, W. B. Muir, B. Heinrich, and Z. Celinski, Phys. Rev. B **42**, 508 (1990).

[21] B. Raquet, M. D. Ortega, A. Sdaq, R. Mamy, M. Goiran, A. R. Fert, C. Armand, and J. C. Ousset, J. Magn. Magn. Mater. **156**, 197 (1996).

[22] J. R. Dutcher, J. F. Cochran, I. Jacob, and W. F. Egelhoff, Jr., Phys. Rev. B **39**, 10 430 (1989).

[23] A. Murayama, K. Hyomi, J. Eickmann, and C. M. Falco, J. Appl. Phys. **83**, 613 (1998).

[24] C. S. Liu and L. J. Chen, Mater. Chem. Phys. **46**, 233 (1996).

[25] F. J. Lamelas, C. H. Lee, Hui He, W. Vavra, and Roy Clarke, Phys. Rev. B **40**, 5837 (1989).

[26] C. H. Lee, Hui He, F. Lamelas, W. Vavra, C. Uher, and Roy Clarke, Phys. Rev. Lett. **62**, 653 (1989).

[27] C. Chappert, K. Le Dang, P. Beauvillain, H. Hurdequint, and D. Renard, Phys. Rev. B **34**, 3192 (1986).

[28] J. F. Cochran, J. M. Rudd, M. From, B. Heinrich, W. Bennett, W. Schwarzacher, and W. F. Egelhoff, Jr., Phys. Rev. B **45**, 4676 (1992).

[29] B. Újfalussy, L. Szunyogh, P. Bruno, and P. Weinberger, Phys. Rev. Lett. **77**, 1805 (1996).

[30] M. Farle, Y. Henry, and K. Ounadjela, Phys. Rev. B **53**, 11 562 (1996).

[31] C. D. England, B. N. Engel, and C. M. Falco, J. Appl. Phys. **69**, 5310 (1991).